Assessing transient changes in the ocean carbon cycle during the last deglaciation through carbon isotope modeling

Hidetaka Kobayashi[1, 2], Akira Oka[2], Takashi Obase[2], and Ayako Abe-Ouchi[2]

[1]Faculty of Science, Academic Assembly, University of Toyama, 3190 Gofuku, Toyama, 930-8555, Japan.
[2]Atmosphere and Ocean Research Institute, University of Tokyo, 5-1-5 Kashiwanoha, Kashiwa, 277-8568, Japan.

Correspondence: H. Kobayashi (hidekoba@sci.u-toyama.ac.jp)

Abstract. We conducted a transient numerical experiment on the ocean carbon cycle during the last deglaciation. We used a three-dimensional ocean field from a transient climate model MIROC4m simulation of the last deglaciation as input to an ocean biogeochemical model, which allowed us to evaluate the effects of the gradual warming and the abrupt climate changes associated with the Atlantic Meridional Overturning Circulation during the last deglaciation.

5   During Heinrich Stadial 1 (HS1), the atmospheric partial pressure of carbon dioxide (pCO_2) increased as a result of rising sea surface temperature. Subsequently, during the Bølling–Allerød period, characterized by a rapid strengthening of the Atlantic Meridional Overturning Circulation (AMOC), atmospheric pCO_2 showed a decreasing trend. Our decomposition analysis indicates that the declining atmospheric pCO_2 in response to the enhanced AMOC during the BA period were primarily driven by an increase in ocean surface alkalinity, although this effect was partially offset by changes in sea surface temperature.

10   Meantime, we found that our model generally underestimated atmospheric pCO_2 changes compared to the ice core data. To understand this, we conducted an analysis of ocean circulation and water masses using radiocarbon and stable carbon isotope signatures ($\Delta^{14}C$ and $\delta^{13}C$). We found that the overall changes in the deep water $\Delta^{14}C$ in response to the AMOC change are quantitatively consistent with the sediment core data. However, the model underestimates the increased ventilation in the deep ocean and the reduced efficiency of biological carbon export in the Southern Ocean during mid-HS1 compared to

15   estimates derived from sediment core data. In addition, the model underestimates the active ventilation in the North Pacific Intermediate Water during mid-HS1, as suggested by sediment core data. These underestimations in the activation of the deep ocean circulation and the limitation of biological productivity could be the primary reasons why our model exhibits smaller atmospheric pCO_2 changes than ice core data.

Our decomposition analysis, which estimates the quantitative contribution to the oceanic pCO_2, suggests that changes in
20   alkalinity have played a central role in driving variations and trends in atmospheric pCO_2 as the deep ocean circulation changes. This finding may provide valuable insights into the model-dependent response of the ocean carbon cycle to changes in the AMOC, as several previous studies have emphasized the importance of the AMOC in influencing changes in atmospheric pCO_2, but the magnitude and direction of these changes have varied widely between studies.

1 Introduction

The Earth's climate has transitioned from the cold climatic conditions of the Last Glacial Maximum (LGM), which is approximately 21,000 years ago, to the warmer Holocene. This climatic transition, known as the last deglaciation, was accompanied by an increase in the atmospheric partial pressure of carbon dioxide (pCO_2) of nearly 90 ppm (Barnola et al., 1987; Petit et al., 1999; Siegenthaler et al., 2005; Jouzel et al., 2007; Lüthi et al., 2008). The changes in the carbon cycle leading to changes in atmospheric pCO_2 are thought to be closely linked to the climate changes that occurred during the deglaciation period.

The concentrations or isotopic composition of elements in seawater provide information on the processes responsible for their distribution. Therefore, analysis of geochemical proxies in paleoclimatological archives can help oceanographers gain insight into past ocean variability and its underlying mechanisms.

Stable and radioactive carbon isotopes of dissolved inorganic carbon (DIC) in seawater are representative chemical tracers in the ocean. In seawater, carbon of lighter isotopes is preferentially absorbed during photosynthesis, leading to its accumulation in the deep ocean as organic matter undergoes degradation (O'Leary, 1981; Broecker and Maier-Reimer, 1992; Schmittner et al., 2013). Therefore, the stable carbon isotopic signature ($\delta^{13}C$) value differs among water masses within the ocean interior. Radiocarbon (^{14}C) is introduced into seawater through gas exchange at the ocean surface and subsequently decreases in concentration as a result of the radioactive decay of ^{14}C. Therefore, the radiocarbon isotopic signature ($\Delta^{14}C$) serves as an indicator of the deep water flow rate (Stuiver et al., 1983). Recent efforts to compile sediment core records have provided valuable insights into the temporal evolution of the basin-scale distributions of $\Delta^{14}C$ (Zhao et al., 2018; Rafter et al., 2022) and $\delta^{13}C$ (Muglia et al., 2023) during the last deglaciation.

Other proxies used to inter past water mass distribution and deep circulation include neodymium isotope ratios (εNd) and protactinium–thorium ratios ($^{231}Pa/^{230}Th$). Neodymium isotope ratios can be used as a proxy for basin-scale water mass structure because the end members differ in each deep water formation region (Howe et al., 2016). Sedimentary $^{231}Pa/^{230}Th$ ratios, employed as a proxy for changes in flow rates, suggest that the strength of the Atlantic Meridional Overturning Circulation (AMOC) may have changed markedly during the last deglaciation (McManus et al., 2004; Ng et al., 2018). Changes in the AMOC influence the climatic state by affecting both meridional interhemispheric heat transport and the ocean carbon cycle, which in turn regulates atmospheric pCO_2 (Schmittner and Galbraith, 2008; Menviel et al., 2008; Bouttes et al., 2012b). Nevertheless, there is an ongoing debate about the magnitude and direction of changes in atmospheric pCO_2 associated with AMOC variations (Gottschalk et al., 2019).

Previous modeling studies examined those processes responsible for changes in the distribution of $\delta^{13}C$ and $\Delta^{14}C$ in glacial oceans (Kurahashi-Nakamura et al., 2017; Menviel et al., 2017; Muglia et al., 2018; Wilmes et al., 2021; Kobayashi et al., 2021). Changes in the efficiency of biological carbon pumps and the deep ocean circulation are recognized as key factors contributing to variations in carbon isotope signatures. However, it is worth noting that previous modeling studies have been somewhat limited in scope, focusing primarily on assessing steady-state differences between the LGM and the preindustrial period. Clarifying the factors behind changes in the distribution of chemical tracers during the glacial termination will improve our understanding of the variability of the ocean carbon cycle and climate during this period.

Transient climate model simulations for the last deglaciation period have been conducted, considering prescribed temporal

60   changes in insolation, greenhouse gas concentrations derived from ice core records, and meltwater fluxes from ice sheets (Lunt et al., 2006; Timm and Timmermann, 2007; Liu et al., 2009; He et al., 2013; Ganopolski and Roche, 2009; Menviel et al., 2011; Ivanovic et al., 2016; Obase and Abe-Ouchi, 2019; Obase et al., 2021; Kapsch et al., 2022; Bouttes et al., 2023). The temporal evolution of the ocean carbon cycle during the last deglaciation has been examined using Earth System Models of Intermediate Complexity (EMIC), e.g., CLIMBER-2 (Bouttes et al., 2012a; Brovkin et al., 2012; Mariotti et al., 2016; Ganopolski and

65   Brovkin, 2017), Bern 3D (Tschumi et al., 2011; Menviel et al., 2012; Pöppelmeier et al., 2023) and LOVECLIM (Menviel et al., 2018; Stein et al., 2020). Other related studies have attempted to estimate variations in the AMOC with respect to meltwater input to the oceans by analyzing changes in carbon isotopic signatures (Schmittner and Lund, 2015; Gu et al., 2021; Pöppelmeier et al., 2023). Generally, the increase in sea surface temperature (SST) and the reduction in the expansion of carbon-rich Antarctic Bottom Water (AABW), along with changes in the characteristics of biological carbon pumps and carbonate

70   chemistry, are considered key processes that contributed to the increase in atmospheric pCO_2 during the last deglaciation (Brovkin et al., 2012; Menviel et al., 2012). Several related studies have suggested that the release of carbon from the deep Southern Ocean to the atmosphere, induced by disruption of the stratification in the Southern Ocean and changes in deep ocean circulation driven by westerly winds in the Southern Hemisphere, freshwater input from the Antarctic ice sheet, and brine rejection around Antarctica, may have been a potential driver of the rapid increase in atmospheric pCO_2 during the

75   last deglaciation (Tschumi et al., 2011; Bouttes et al., 2012a; Mariotti et al., 2016; Menviel et al., 2018; Stein et al., 2020; Sigman et al., 2021; Gray et al., 2023; Sikes et al., 2023). It is also suggested that variation of the North Pacific Intermediate Water (NPIW), associated with changes in the circulation of the Atlantic Ocean, may have contributed to the increase in atmospheric pCO_2 (Okazaki et al., 2010; Menviel et al., 2014). Some of these EMIC studies have discussed the mechanisms of deglacial changes in the ocean carbon cycle by conducting model–data comparisons of carbon isotope signatures. However,

80   these discussions are limited to the vertical one-dimensional distribution of these signatures.

To investigate the causes of changes in carbon isotope signatures, this study conducted a transient model experiment of the ocean carbon cycle and compared the model results with a compiled sediment core record. Additionally, the factors responsible for changes in atmospheric pCO_2 resulting from variation in ocean carbon storage were analyzed. The objective of this study is to gain a better understanding of the processes contributing to changes in the deglacial carbon cycle through these efforts.

85   2   Methods

2.1   Model

This study performed numerical experiments by coupling an ocean biogeochemical tracer model based on Parekh et al. (2005) with the CCSR Ocean Component Model version 4.0 (Hasumi, 2006) to evaluate the transient response of the global ocean carbon cycle during the last deglaciation. The horizontal resolution of the model was approximately 1 degree, and it had 44

90   vertical layers (5–250 m). The boundary condition of the ocean biogeochemical cycle model was the monthly averaged output of a climate model simulation focused on the last deglaciation (Obase and Abe-Ouchi, 2019; Obase et al., 2021) performed

using an atmosphere–ocean general circulation model (AOGCM), i.e., MIROC 4m (K-1 Model Developers, 2004), incorporating horizontal advection velocity, sea surface height, vertical diffusivity, temperature, salinity, shortwave radiation, wind speed above the sea surface, and sea ice concentration. The prognostic variables for the ocean biogeochemical model were phosphate,

95 DIC, alkalinity, dissolved organic phosphate, dissolved oxygen, iron, silicate, and carbon isotopes of DIC (^{13}C and ^{14}C). The availability of light, phosphate, and iron was used to determine the rate of phosphate uptake by phytoplankton. Sedimentation processes on the seafloor were not considered, and all particles reaching the seafloor were assumed to dissolve in the deepest layer of the model.

2.2 Experimental design

100 We conducted ocean carbon cycle experiments for the last deglaciation spanning from 21 to 11 thousand years before present (kaBP).

2.2.1 Steady-state experiment for the Last Glacial Maximum

To obtain the initial state of the deglaciation experiment, the ocean biogeochemical cycle model was spun up under the LGM ocean state (21 kaBP) calculated by the AOGCM. Dust deposition to the ocean surface was taken from a simulation of the

105 SPRINTARS aerosol transport–radiation model computed under LGM climatic conditions (Takemura, 2005). We assumed iron deposition at the sea surface to be 3.5 wt% of the total dust deposition, with an assumed iron solubility of 1% (Parekh et al., 2005). The initial distribution of ocean biogeochemical tracers was taken from the climatology of the World Ocean Atlas 2001 (Conkright et al., 2002; Locarnini et al., 2002) and the Global Ocean Data Analysis Project (Key et al., 2004). The initial iron concentration was set to a constant value of 0.6 nmol. The model was initialized with values of atmospheric δ^{13}C and

110 Δ^{14}C at 21 kaBP of -6.5‰ and 0‰ respectively.

Notably, the biogeochemical cycle simulation of the LGM ocean performed in this study did not include certain processes such as enhanced Southern Ocean stratification, iron fertilization from glaciogenic dust, and carbonate compensation, as discussed in Kobayashi et al. (2021). These three processes were found to contribute to the reduction in atmospheric pCO$_2$ in our previous studies, and therefore the calculated atmospheric pCO$_2$ during the LGM was expected to be higher than the at-

115 mospheric pCO$_2$ reported in Kobayashi et al. (2021). Additional ocean general circulation model experiments are needed to obtain the physical ocean fields that account for the enhanced Southern Ocean stratification; therefore, this process could not be incorporated into the current model setup.

2.2.2 Transient experiment during the last deglaciation

A transient experiment was conducted to investigate the ocean biogeochemical cycle during the last deglaciation, starting from

120 the initial state of the LGM. The temporal variations in temperature and the AMOC in the output of the AOGCM imposed on the boundary conditions are shown in Fig. 1. During the transient experiment, dust deposition was periodically adjusted every 100 years based on the scaling between the LGM and the Holocene, using the reconstructed dust deposition from the Dome Fuji

ice core (Dome Fuji Ice Core Project Members, 2017). Notably, the transient experiment did not consider temporal variation in the ocean volume or the changes in dissolved matter concentration induced by ocean volume change. This simplification will

125   be revised in the future.

We also predicted the ^{13}C and ^{14}C contained in atmospheric CO_2. After the spin up of the LGM ocean, we determined the restoring term to prevent drift in δ^{13}C and Δ^{14}C in the atmosphere due to gas exchange between the atmosphere and the ocean. The restoring term implies exchange of carbon isotopes between the atmosphere and the land, together with the production of ^{14}C in the atmosphere. This restoring term was assumed to remain unchanged throughout the deglaciation experiment.

130   ## 3   Results

3.1   Ocean carbon cycle during the LGM time-slice

Figure 2 shows the calculated temporal variations in Δ^{14}C-CO_2, δ^{13}C-CO_2, and pCO_2 in the atmosphere (solid line), together with their reconstructed estimate (dashed line). Figure 2 also shows temporal variations in the average of $\Delta\Delta^{14}$C, which are the differences in Δ^{14}C between the ocean and the atmosphere, δ^{13}C, and DIC in the middle (500–2000 m) and deep (> 2000 m)

135   layers of the Atlantic, Southern (< 40° S), and Pacific oceans. In response to changes in the climate and the deep ocean circulation during the deglaciation, the ocean carbon cycle is altered.

First, we discuss the differences between the LGM and the Holocene. Our climate model experiment indicates a weaker AMOC during the LGM (21 kaBP) compared to that in the Holocene (11 kaBP) (Figs. 1a and S1). The basin-wide distributions of $\Delta\Delta^{14}$C and δ^{13}C in the Atlantic and Pacific oceans at specific time periods are presented in Figs. 3 and 4. The model results

140   demonstrate that $\Delta\Delta^{14}$C, an indicator of ocean ventilation, is lower in the deep Atlantic at 21 kaBP than at 11 kaBP (Figs. 2c, 3a and f), which is in qualitative agreement with reconstructions from sediment core records (Rafter et al., 2022). Notably, however, the model experiment underestimates the reconstruction of $\Delta\Delta^{14}$C at 21 kaBP in the Atlantic below 3000 m and in the Pacific below 2000 m (Fig. 3a). Regarding δ^{13}C, the model results show a stronger vertical gradient between the surface and deep ocean in the Atlantic (Fig. 2h), corresponding to a shallower and weaker AMOC at 21 kaBP compared to that at

145   11 kaBP. This qualitative difference is consistent with the reconstructed δ^{13}C. However, similar to the finding for $\Delta\Delta^{14}$C, our model experiment underestimates the reconstruction of δ^{13}C in the deep ocean, particularly in the Southern and Pacific oceans (Figs. 2i and j). Our previous study, which involved numerical experiments under LGM conditions that accounted for the enhanced stratification in the Southern Ocean and iron fertilization from glaciogenic dust, showed improved quantitative agreement between the model and sediment core data for dissolved oxygen, δ^{13}C, and Δ^{14}C (Kobayashi et al., 2021). The

150   triangles in Fig. 2 illustrate the changes in the carbon isotope signatures reported in that study. A comparison of the two studies suggests that the absence of these processes is a major factor in the underestimation of changes in the carbon isotope signatures in the deep ocean.

Atmospheric pCO_2 was predicted by running the ocean carbon cycle model. Its value was 278.1 ppm at 21 kaBP and 306.9 ppm at 11 kaBP, i.e., a difference of 28.8 ppm, which is relatively small compared with the difference of approxi-

155   mately 80 ppm reconstructed from ice cores (approximately 188 to 267 ppm in EPICA Dome C (Bereiter et al., 2015) and

approximately 193 to 273 ppm in WAIS Divide (Bauska et al., 2021)). One possible explanation for this discrepancy is the relatively small difference in SST between the two intervals in our experiment (Fig. 1b). Previous studies using proxy and data assimilation reported a global mean SST difference between the LGM and the Holocene of 1.7 to 3.6 °C (MARGO Project Members, 2009; Tierney et al., 2020; Paul et al., 2021; Annan et al., 2022), whereas the SST difference in our experiment was

160 only 1.6 °C. A small difference in SST leads to a small difference in CO_2 solubility between the two periods, resulting in underestimation of the amplitude of the atmospheric pCO_2. Another possible reason is that the specific processes that contributed to the lower atmospheric pCO_2 introduced in Kobayashi et al. (2021), i.e., enhanced salinity stratification, iron fertilization from glaciogenic dust, and carbonate compensation, were not considered in this study. The differences in the steady-state ocean carbon cycles at 21 and 11 kaBP highlight the difficulty in accurately reproducing the actual changes in atmospheric

165 pCO_2 in the transient experiment connecting these periods. Therefore, our analysis focuses on investigation of the impacts of climate change, particularly the notable variations in the AMOC, on the ocean carbon cycle, and reveals model successes and deficiencies through model–data comparison of carbon isotope signatures.

3.2 Basin-scale changes in carbon isotopes during the last deglaciation

3.2.1 Radiocarbon isotopes

170 Here, we present the transient changes in the ocean carbon cycle during the last deglaciation. During the deglaciation, atmospheric $\Delta^{14}C$ was reported to decrease from approximately 500‰ to 0‰ (Fig. 2a). Seawater $\Delta\Delta^{14}C$ generally increases from a relatively low LGM value, although it might decrease at times (Figs. 2b–e). Generally, the state of the AMOC strongly influences the distribution of $\Delta\Delta^{14}C$. Both the model and the sediment core records show an increase in $\Delta\Delta^{14}C$ in the deep ocean during periods when the AMOC is relatively strong, e.g., the Bølling–Allerød (BA) and Holocene, and a decrease in $\Delta\Delta^{14}C$

175 during periods when the AMOC is relatively weak, e.g., Heinrich Stadial 1 (HS1) and the Younger Dryas (YD). During the BA and Holocene, the zonal mean of $\Delta\Delta^{14}C$ remains above -200‰ throughout the Atlantic owing to active ventilation (Figs. 3d and f). Conversely, when the AMOC is relatively weak, the zonal mean of $\Delta\Delta^{14}C$ decreases to values below -200‰ in the deep ocean and the Southern Ocean, particularly during HS1 (Figs. 3b and c). The pattern of changes in $\Delta\Delta^{14}C$ induced by the changes in the AMOC is consistent with the pattern seen in the sediment core records.

180 In the Pacific, when the AMOC is strong (i.e., at 13 and 11 kaBP), the $\Delta\Delta^{14}C$ in the South Pacific is relatively high, with elevated values from the surface to the deep Southern Ocean along the path of the AABW. Some sediment core records compiled in Rafter et al. (2022) indicate elevated $\Delta\Delta^{14}C$ at depths near 1000 m during HS1, possibly indicating the influence of NPIW intrusion. However, the model results do not provide clear indication of the intrusion of young water masses.

The compiled sediment core records demonstrate substantial increase globally in $\Delta\Delta^{14}C$ during HS1, whereas the model

185 experiment does not show such pronounced change (Figs. 2b–e). This discrepancy can be attributed to the fact that the model experiment did not accurately simulate the variations in ocean carbon storage, as reflected in the atmospheric pCO_2 (Fig. 2k). In other words, considering the glacial–interglacial redistribution of carbon in the atmosphere–ocean system, the relative

abundances of ^{14}C to ^{12}C in the atmosphere are higher during the ice age, as manifested in the atmospheric $\Delta^{14}C$-CO_2 (Fig. 2a), but the variation in ^{12}C is not well reproduced in the model experiment (Fig. 2k).

190   The triangles shown in Fig. 2 represent the results of the best LGM simulation (LGM_all) conducted by Kobayashi et al. (2021). That simulation incorporated enhanced salinity stratification and sedimentation processes, which further contribute to accurate reproduction of low $\Delta\Delta^{14}C$ deep water during the LGM. As shown in Figs. 2b–e, there is substantial discrepancy between the model and the reconstruction, particularly in the Southern Ocean during the period of early deglaciation. The incorporation of changes in vertical mixing, resulting from variations in ocean stratification, could potentially improve the

195   $\Delta^{14}C$ simulation during the deglaciation.

3.2.2   Stable carbon isotopes

Next, we focus on the changes in $\delta^{13}C$. For seawater $\delta^{13}C$, the overall trends of change for $\delta^{13}C$ and $\Delta\Delta^{14}C$ are similar and correspond to phases of climate change; however, $\delta^{13}C$ is less sensitive than $\Delta\Delta^{14}C$ to climate change (Fig. 2). This could be associated with biological fractionation. With a stronger AMOC, more light carbon is transported to deeper layers, especially

200   in the North Atlantic, due to increased biological production. This counteracts the effect of lighter carbon being transported to the surface by the active AMOC.

During HS1, the AABW extends from the Southern Ocean into the deep ocean with relatively low $\delta^{13}C$ endmembers compared to the North Atlantic Deep Water (NADW), leading to reduction in $\delta^{13}C$ at approximately 3000 m in the North Atlantic, consistent with the reconstructed data (Fig. 2h). The data clearly show an increase in $\delta^{13}C$ in the mid–deep Southern

205   Ocean (Figs. 2i and 4a–c). This change suggests loss of light carbon accumulated via biological processes during HS1; however, this trend was not quantitatively simulated in the model.

During the BA (Fig. 4d) and Holocene (Fig. 4f), when the AMOC is intensified, high $\delta^{13}C$ originating from the North Atlantic Ocean expands into the deep ocean at depths below 2000 m. The reconstructed basin-averaged $\delta^{13}C$ also shows increase in $\delta^{13}C$ in the deep ocean during the BA (Figs. 2g–j). However, the data do not show further reduction in $\delta^{13}C$ in the

210   deep ocean during the YD, which is different from the calculated change.

Changes in $\delta^{13}C$ in these deeper layers are also reflected in atmospheric $\delta^{13}C$-CO_2. Atmospheric $\delta^{13}C$-CO_2 has a sharp drop during HS1, it then rises slightly during the BA, before falling again during the YD, whereas the model-calculated changes in the ocean carbon cycle do not reproduce such a trend in atmospheric $\delta^{13}C$-CO_2 (Fig. 2f). The discrepancy between the model and data may be due to the contribution of vegetation. This will be discussed later.

215   In addition to changes in the deep ocean circulation, isotope fractionation by temperature-dependent gas exchange and by phytoplankton, which preferentially takes up lighter carbon, is also an important factor for $\delta^{13}C$ variation. Figure S6 shows the calculated changes in organic carbon export from that in 21 kaBP with qualitative changes in biological flux reconstructed from proxies, specifically opal flux and alkenone flux, in sediment core records (Chase et al., 2003; Anderson et al., 2009; Bolton et al., 2011; Kohfeld and Chase, 2011; Martínez-García et al., 2014; Maier et al., 2015; Studer et al., 2015; Thiagarajan

220   and McManus, 2019; Ai et al., 2020; Weber, 2021; Li et al., 2022). During HS1, both the models and the proxies show increased biological carbon transport in the Southern Hemisphere polar regions (Figs. S6a–d). In the polar regions, sea ice is

reduced owing to warming, which could result in less light limitation and allow increased biological productivity. During HS1, biological carbon transport is reduced in the subpolar region and in the South Pacific gyres. These changes in the southern regions can be attributed to reduced nutrient supply resulting from weakening of the AMOC. Another important factor is the

225   increased iron limitation associated with the reduced supply of dust-derived iron that affects biological production. During the BA warm period, the enhanced AMOC enhances nutrient transport from the deep to the surface ocean, resulting in increased biological transport in the North Atlantic (Figs. S6e and f). These changes in nutrient transport then propagate to the North Pacific. From the BA to YD, there is an increase in biological exports in the Southern Ocean, which may be attributed to a reduction in sea ice as a result of warming in the Southern Hemisphere. The factors that alter biological production in the

230   model are understood, but need to be constrained from additional proxy data with high temporal resolution that can capture of millennial-scale variation.

3.3   Changes in atmospheric $p\text{CO}_2$ during the last deglaciation caused by changes in the ocean carbon cycle

Figure 2k shows the calculated changes in atmospheric $p\text{CO}_2$ driven by climate and carbon cycle changes during the last deglaciation. To investigate those factors driving the change in atmospheric $p\text{CO}_2$, we decomposed the factors relevant to

235   the partial pressure of CO_2 at the sea surface ($p\text{CO}_2{}^{os}$). This parameter controls atmospheric $p\text{CO}_2$ through gas exchange between the atmosphere and the ocean. Oceanic $p\text{CO}_2$ is influenced by temperature, salinity, DIC, and alkalinity, which are factors related through the carbonate system. The impact of those factors on $p\text{CO}_2{}^{os}$ can be represented as follows:

$$p\text{CO}_2{}^{os} = f(\text{sDIC}, \text{sALK}, \text{SST}, \text{SSS}) \tag{1}$$

where sDIC is sea surface DIC, sALK is sea surface alkalinity, SST is sea surface temperature, and SSS is sea surface salinity. The function f is determined based on the inorganic chemistry of the carbonate system (Millero, 1995). By analyzing the

240   changes in each variable from their original values, we can determine the contribution of each factor to the variation in $p\text{CO}_2{}^{os}$.

3.3.1   Heinrich Stadial 1

During HS1, atmospheric $p\text{CO}_2$ rose slightly to approximately 17 kaBP, then rose sharply to approximately 15 kaBP. From 18 to 15 kaBP, atmospheric $p\text{CO}_2$ increased by $10.2\ \text{ppm}$ (Fig. 5a), whereas the WAIS Divide ice core record shows an increase of $41.4\ \text{ppm}$ during the same period (Bauska et al., 2021). The model accounted for approximately one quarter of

245   the reconstructed changes in atmospheric $p\text{CO}_2$. Decomposition analysis of $p\text{CO}_2{}^{os}$ revealed that most of the variation in $p\text{CO}_2{}^{os}$ is driven by changes in SST (Figs. 5a and b). Figures S7b and c show the changes in $p\text{CO}_2{}^{os}$ ($\Delta p\text{CO}_2{}^{os}$) attributable solely to variations in both temperature and salinity ($\Delta p\text{CO}_2{}^{os}(\text{TS})$) and DIC and alkalinity ($\Delta p\text{CO}_2{}^{os}(\text{CA})$). It is evident that $\Delta p\text{CO}_2{}^{os}(\text{TS})$ shows a predominantly positive contribution globally, reflecting the pattern of SST increase (Fig. S7d), because increasing SST reduces CO_2 solubility. In other words, the main contributor to the $p\text{CO}_2{}^{os}$ increase during HS1 is warming,

250   especially in the subantarctic region.

3.3.2 Bølling-Allerød

At the onset of the BA transition near 14.7 kaBP, atmospheric $p\text{CO}_2$ began to decrease, and this reduction continued until 12.8 kaBP (Fig. 2k). During the BA period, the contributions of thermal changes and geochemical changes acted in opposition to the change in atmospheric $p\text{CO}_2$ (Figs. 5c and d). At the onset of the BA, as the AMOC strengthened (Fig. 1a), SST and

255 SSS both increased in the Northern Hemisphere and decreased in the Southern Hemisphere (Fig. S8d). The net contribution of $p\text{CO}_2{}^{os}$(TS) attributable to changes in CO_2 solubility was positive (Figs. 5c and d). On the other hand, the enhanced AMOC facilitates the transport of nutrients, carbon, and alkalinity from the deep to the surface ocean, especially in the North Atlantic (Figs. S8e and f). The increase in sDIC leads to an increase in $p\text{CO}_2{}^{os}$, while the increase in sALK leads to a reduction in $p\text{CO}_2{}^{os}$. These opposing effects partially offset each other, resulting in net reduction in $p\text{CO}_2{}^{os}$ (Figs. 5c, 5d, and S8c).

260 Additionally, as the AMOC resumed over time, increased biological production in most of the global ocean led to a millennial-scale decrease in sDIC, contributing to decrease in $p\text{CO}_2{}^{os}$ (Figs. 5c and d). In summary, following the recovery of the AMOC, the opposing contributions of $\Delta p\text{CO}_2{}^{os}$(TS) and $\Delta p\text{CO}_2{}^{os}$(CA) to $\Delta p\text{CO}_2{}^{os}$ over time controlled the temporal changes in $p\text{CO}_2{}^{os}$ and subsequent reduction in atmospheric $p\text{CO}_2$.

3.3.3 Younger Dryas

265 Atmospheric $p\text{CO}_2$ rose again at the onset of the YD period (12.8 kaBP), coinciding with the collapse of the AMOC into a weak state (Fig. 1a). Decomposition analysis of $p\text{CO}_2{}^{os}$ revealed that the influences of $\Delta p\text{CO}_2{}^{os}$(TS) and $\Delta p\text{CO}_2{}^{os}$(CA) on the overall $\Delta p\text{CO}_2{}^{os}$ were in opposite directions. This offset is also observed during the BA, but in the opposite sense. The contribution of $\Delta p\text{CO}_2{}^{os}$(TS) increased over time, leading to an increase in $p\text{CO}_2{}^{os}$ (Figs. 5e and f). The contribution of $\Delta p\text{CO}_2{}^{os}$(CA) was small. As the AMOC weakened, reduction in sALK contributed to an increase in $p\text{CO}_2{}^{os}$, but the decrease

270 in sDIC contributed to a reduction in $p\text{CO}_2{}^{os}$ (Figs. 5e and f, and S9c, e, and f). Consequently, $p\text{CO}_2{}^{os}$ decreased slightly during the YD.

4 Discussion

This study investigated the transient response of the ocean carbon cycle during the last deglaciation. By comparing the calculated carbon isotope signatures of $\delta^{13}\text{C}$ and $\Delta^{14}\text{C}$ with those of sediment core records, we can identify potential biases and

275 errors in the model, as well as examine the impacts of climate and AMOC changes on those signatures. The simulation of carbon isotope signatures in addition to atmospheric $p\text{CO}_2$ contributes to a comprehensive understanding of past changes in the global carbon cycle.

4.1 Response of carbon isotope signatures to drastic changes in the deep ocean circulation

Comparing the changes in $\Delta\Delta^{14}\text{C}$ between models and data allows us to evaluate the accuracy of the computed AMOC

280 variations. The variations in $\Delta\Delta^{14}\text{C}$ regarding the notable shifts in the AMOC after the BA transition are generally consistent

with the reconstruction. Corresponding to the AMOC change, $\Delta\Delta^{14}C$ increases in the deep ocean from the deep Atlantic to the Pacific Ocean (Figs. 2c–e). Subsequently, $\Delta\Delta^{14}C$ decreased from the Atlantic Ocean to the Southern Ocean during the YD in response to the weakening of AMOC. This change is consistent with the reconstruction, but the quantitative changes in the deep ocean are overestimated (Fig. 3e). This may be related to the reproducibility of the ocean circulation fields, which will be

285   discussed below.

Pöppelmeier et al. (2023) use Bern3D model to estimate AMOC changes during the last deglaciation from multiple model–data comparisons between carbon isotope ratios, εNd, and $^{231}Pa/^{230}Th$. Their research suggests that the AMOC gradually weakens during HS1, recovers at the BA transition, and weakens again during the YD, but it does not completely collapse. This proposed pattern of AMOC change is qualitatively consistent with our ocean modeling of Obase and Abe-Ouchi (2019) (Fig.

290   1a). The Bern3D study also shows that the proportion of deep water originating from the North Atlantic is not much different from that during the BA because of the short duration of the YD period. In contrast, this study shows that the distribution of $\Delta^{14}C$ and $\delta^{13}C$ changes almost completely at the basin scale in response to changes in the AMOC over approximately 1000 years (Figs. 3 and 4). Our model indicates a longer period of relatively weak AMOC during the YD compared to the Bern3D model, which helps to explain the discrepancies between the model and data in the deep North Atlantic during the

295   YD. However, it is important to recognize that even with similarities in AMOC strength changes, there are differences in the overall deep ocean circulation field, including the AABW, between models, resulting in differences in basin-scale chemical tracer changes. Since each model has systematic biases in physical and biogeochemical processes, it is valuable to compare multiple models to explore realistic AMOC variations in the past. The importance of this study is that it examines how the AMOC mode change affects the three-dimensional structure of water masses, not only in the Atlantic, but also in the Southern

300   and Pacific oceans.

For $\delta^{13}C$, the model and data show the same trend of an increase in deep water $\delta^{13}C$ during the BA as $\Delta\Delta^{14}C$. After that, the model shows a decrease in deep water $\delta^{13}C$ during the YD, but the reconstruction does not show this feature (Figs. 2g–j). The mismatch is particularly pronounced from the Southern Ocean to the deep ocean. Possible contributing factors include variations in the signal of change and dating errors in individual sediment data. Another factor is that not only ocean

305   circulation but also ecosystem responses are not adequately reproduced. The calculated export of biogenic organic matter in the Southern Ocean increased during the YD period compared to the BA period (Figs. S6f and g), resulting in a decrease in $\delta^{13}C$ from the Southern Ocean to the deep ocean. This biological response demonstrates that, without this change, a decrease in $\delta^{13}C$ would not be observed in the deep ocean. Since a decrease in nutrient concentrations limits biological productivity, it is crucial to accurately simulate the nutrient and iron cycles associated with nutrient limitation of biological productivity. In

310   particular, as the Southern Hemisphere warms and becomes more humid, the supply of iron from dust may decrease (Martin, 1990; Martínez-García et al., 2014). This change has a substantial impact on ocean productivity in iron-limited regions, which subsequently affects atmospheric pCO$_2$. The interpretation of discrepancies between models and data on $\delta^{13}C$ changes is an open question.

4.2 Insights from carbon isotope ratios: CO_2 release from the ocean to the atmosphere

315   Ocean modeling with freshwater forcing experiments has provided insight into the link between the shutdown and resumption of the AMOC and changes in atmospheric pCO_2. Schmittner and Galbraith (2008) showed that cessation of the AMOC leads to an increase in atmospheric pCO_2, which is due to several factors. The efficiency of the biological carbon pumps in NADW is relatively high compared with that in AABW, and therefore the reduced inflow of NADW leads to reduction in biological carbon sequestration in the deep ocean. Moreover, weakening of the Southern Ocean stratification, associated with AMOC

320   shutdown, increases the outgassing of CO_2 from the ocean to the atmosphere. This study confirms the gradual increase in atmospheric pCO_2 during HS1 and YD in parallel with the AMOC weakening, but such an increase is not directly related to a reduction in the regenerated nutrient inventory, as suggested by Schmittner and Galbraith (2008). The reason for this difference is that the contribution of the change in alkalinity to the change in pCO_2^{os} during the YD was greater than the contribution of the change in DIC in this study. When the AMOC changes, the resulting atmospheric pCO_2 anomaly depends on the magnitude

325   of the relative contributions of DIC and alkalinity to pCO_2^{os}, based on the vertical gradient of DIC and alkalinity between the surface and deeper ocean. While the pCO_2 response varies depending on the model used and the initial distribution of DIC and alkalinity, this study shows that increased SST and reduced surface ocean alkalinity emerge as major contributors to the deglacial increase in atmospheric pCO_2.

   Simulating changes in $\Delta\Delta^{14}C$ during the early deglaciation is challenging. During HS1, the sediment core records show

330   that $\Delta\Delta^{14}C$ increased by $200‰$ in the deep Southern Ocean and by $100‰$ in other deep oceans (Figs. 2c–e). The idea that ventilation increased during HS1 and that CO_2 was released from the oceans into the atmosphere is consistent with the increase in atmospheric pCO_2 during this period. In contrast, the current model cannot fully reproduce the large changes in ventilation. The process that may be involved in this change in ventilation during HS1 is discussed below.

   Ice core reconstructions show that atmospheric $\delta^{13}C$-CO_2 is depleted during HS1, but the calculated $\delta^{13}C$-CO_2 variations

335   are insufficient in terms of its amplitude (Fig. 2f). One factor is the limited amplitude of the ventilation change, as evidenced by the change in $\Delta\Delta^{14}C$, because the upwelling of light carbon to the upper layers and its exchange between the ocean and the atmosphere lead to a reduction in atmospheric $\delta^{13}C$-CO_2. In Kobayashi et al. (2021), iron fertilization from glaciogenic dust was shown to increase biological production in the subantarctic region, which contributed to the reproduction of low $\delta^{13}C$ in the deep Southern Ocean during the LGM. Their study does not reproduce the extremely old water suggested by radiocarbon

340   in the deep glacial Southern Ocean (triangles in Fig. 2d), but it does reproduce low $\delta^{13}C$ (triangles in Fig. 2i). The change in glaciogenic dust deposition was not considered in this study, and therefore the model might underestimate the variation in biological production in the subantarctic region, which might contribute to underestimation of the changes in atmospheric and deep-sea $\delta^{13}C$ during HS1. In future efforts to reproduce the carbon cycle during HS1, the model–data comparison of $\Delta\Delta^{14}C$ and $\delta^{13}C$ shows that it is important to reproduce both the activation of ventilation and the changes in biological production,

345   including the strengthening of iron limitation in the Southern Ocean.

   Besides, in the North Pacific, the sediment core records show increase in $\Delta\Delta^{14}C$ near $1000\,\mathrm{m}$ during HS1 (Okazaki et al., 2010; Rae et al., 2014; Rafter et al., 2022). The NPIW was suggested to be strengthened or deepened during HS1, but this

change is only partially explained by the calculated changes in $\Delta\Delta^{14}C$. By analyzing radiocarbon and boron isotopes in sediment cores, Rae et al. (2014) show that the NPIW expanded during HS1. Using an EMIC of GENIE, they show that

350   these ventilation changes contribute to an increase in atmospheric $p\mathrm{CO}_2$. Chikamoto et al. (2012) compared an AOGCM of MIROC, the model we use, with an EMIC of LOVECLIM. They show that both models concur on the activation of the NPIW when freshwater flows into the North Atlantic. However, it is also indicated that the response of the ocean circulation is less pronounced in MIROC. The activation of the ocean circulation and the degassing of CO_2 in the North Pacific during the early deglaciation are processes that have the potential to contribute to the currently unexplained increase in atmospheric $p\mathrm{CO}_2$.

355   High-resolution ice core data from the WAIS Divide provide valuable insights into the changes in atmospheric $p\mathrm{CO}_2$ during the last deglaciation. It is suggested that there are two modes of change in atmospheric $p\mathrm{CO}_2$: slow increase on the millennial scale and rapid increase on the centennial scale (Marcott et al., 2014). The rapid increase in atmospheric $p\mathrm{CO}_2$ of 10–15 ppm at the end HS1 (14.8 kaBP) and at the end of YD (11.7 kaBP) over a short period of 100–200 years, synchronized with the resumption of the AMOC (McManus et al., 2004; Ng et al., 2018). However, this study did not reproduce such abrupt

360   changes in atmospheric $p\mathrm{CO}_2$. Several factors might contribute to this discrepancy, including insufficient temperature rise in the Southern Hemisphere associated with AMOC changes, inadequate representation of the vertical concentration gradients of DIC and alkalinity, limitations in capturing atmospheric and oceanic dynamics in the general circulation model, and the influence of small-scale phenomena. Previous modeling studies have suggested that deeper convection in the Southern Ocean and a strengthening of westerly winds in the Southern Hemisphere could contribute to the abrupt jump in atmospheric $p\mathrm{CO}_2$

365   during the middle of HS1 (16.3 kaBP) by transporting sequestered carbon from the deep Southern Ocean to the surface (Menviel et al., 2018). Since these processes are related to the challenges in reproducing carbon isotope ratios described earlier, these results suggest that our AOGCM and its experimental setup need to be improved.

4.3   Implications for future improvements to the model and experimental design

Model–data comparisons of carbon isotope signatures underscore the importance of refining our climate models to more

370   accurately represent the complex interactions that govern changes in the carbon cycle. Future improvements to the AOGCM may include the following considerations.

For example, the AOGCM used in this study did not account for temporal changes in the ice sheet and underestimated the Southern Ocean SST changes (Obase and Abe-Ouchi, 2019). There is some uncertainty as to how much meltwater has flowed across the North Atlantic during HS1 (Ivanovic et al., 2018; Snoll et al., 2023) and BA (Kapsch et al., 2022; Bouttes et al.,

375   2023). This suggests that the problem persists within the AOGCM, where the model's AMOC response is not consistently realistically reproduced, even when realistic freshwater variations are applied. Furthermore, as shown in Obase et al. (2023), the magnitude of ocean warming during the deglaciation varies depending on the response characteristics of each model, resulting in a range across multiple models. Sherriff-Tadano et al. (2023) demonstrated that altering parameters associated with cloud thermodynamic phase fractions in a climate model mitigates warming biases of SST in the modern Southern Ocean.

380   Using a model with reduced Southern Ocean warming bias is expected to yield different responses in Southern Ocean SST and ocean circulation during the glacial period, as well as in their changes during the deglaciation, compared to this study.

Furthermore, although some studies propose potential alterations in the westerly winds over the Southern Ocean throughout the deglaciation (Gray et al., 2023), there is a substantial degree of uncertainty concerning the anticipated changes in atmospheric dynamics during the deglaciation. These uncertainties could have a substantial impact on the results of ocean biogeochemical models and, consequently, on atmospheric $p\mathrm{CO_2}$. Efforts to mitigate biases and facilitate a comprehensive discussion of climate model coherence are critical to advancing future climate-carbon cycle modeling. These endeavors are essential to refine our understanding of the complex interactions between climate and the carbon cycle.

In addition to those factors mentioned above, there are several other factors that could contribute to improving the simulation of the ocean carbon cycle during the period of the last deglaciation. One important consideration is the inclusion of critical processes for lowing atmospheric $p\mathrm{CO_2}$ during the LGM, which were identified in Kobayashi et al. (2021). Those processes include enhanced stratification of the Southern Ocean, iron fertilization from glaciogenic dust, and carbonate compensation. Understanding the changes in those processes during the deglaciation is critical, and properly incorporating them into future modeling efforts might lead to improved simulations and better understanding of the dynamics during this period. In addition, it has been reported that the inclusion of a parameterization of vertical mixing that depends on the tidal mixing energy and stratification can better reproduce the Pacific circulation (Oka and Niwa, 2013; Kawasaki et al., 2022). The introduction of tidal mixing parameterization has also proven effective in reproducing $\delta^{13}\mathrm{C}$ and $\Delta^{14}\mathrm{C}$ in the glacial ocean (Wilmes et al., 2021). Incorporating the insights from these model development has the potential to lead to a more realistic representation of carbon cycle variations during the glacial period and subsequent deglaciation.

Furthermore, it is worth noting that carbon exchange between the atmosphere and the ocean is not the sole driver of deglacial variation in atmospheric $p\mathrm{CO_2}$. Changes in terrestrial and soil carbon storage also play important roles in modulating atmospheric $\delta^{13}\mathrm{C}$ and $p\mathrm{CO_2}$ during the deglaciation (Schmitt et al., 2012; Bauska et al., 2021). Trends in atmospheric $\delta^{13}\mathrm{C}$-$\mathrm{CO_2}$ changes differ between the reconstruction and the model (Fig. 2f). The model shows that, contrary to the reconstruction, atmospheric $\delta^{13}\mathrm{C}$-$\mathrm{CO_2}$ decreases during the BA and increases during the YD. A possible explanatory factor, in addition to the challenges of reproducing biological productivity mentioned above, is that there is a lack of preferential uptake of light carbon by terrestrial vegetation. Comparison of $\Delta^{14}\mathrm{C}$-$\mathrm{CO_2}$ and $\delta^{13}\mathrm{C}$-$\mathrm{CO_2}$ provides a consistent explanation if carbon uptake by vegetation expands during the BA and declines during the YD as suggested by Schmitt et al. (2012). Vegetation growth, driven by $\mathrm{CO_2}$ fertilization, can act as a sink for $\mathrm{CO_2}$ and counteract the rise in atmospheric $p\mathrm{CO_2}$ (Bouttes et al., 2012a; Menviel et al., 2012). Therefore, it may be possible to revisit the changes in atmospheric $p\mathrm{CO_2}$ during the BA and YD periods that were described by the ocean-only processes in this study. Future studies using Earth system models that include both terrestrial and oceanic carbon cycle processes would contribute to more comprehensive understanding of glacial changes in carbon cycles. A study of the carbon cycle associated with the glacial Dansgaard–Oeschger events has been conducted in an ESM of CESM1 and has shown that at this time scale, changes in terrestrial carbon storage are as important as those in the oceans (Jochum et al., 2022). Moreover, in previous studies using EMICs, temporal variations in atmospheric $p\mathrm{CO_2}$ are primarily used to calculate changes in radiative forcing, and several studies have explored the interaction between the carbon cycle and climate (Bouttes et al., 2012a; Ganopolski and Brovkin, 2017). Although fully coupling a carbon cycle model with a climate model is a more advanced endeavor, we are interested in pursuing such research.

5   Conclusions

To understand the mechanisms of glacial–interglacial variability in the carbon cycle, this study focused on the last deglaciation period and investigated the transient response of the ocean carbon cycle to climate change, including the significant strengthening and weakening of the AMOC.

Our model qualitatively simulates an increase in atmospheric pCO_2 during HS1. The calculated atmospheric pCO_2 increase was found to be caused by an increase in SST. The relatively modest increase in atmospheric pCO_2, compared with that of the ice core record, might be attributable in part to relatively small increases in SST in the Southern Ocean. Furthermore, model–data comparisons of carbon isotope signatures suggest that the model inaccurately represents the increased ventilation in the deep ocean and the decreased efficiency of surface biological productivity in the Southern Ocean and underestimates the activation of the NPIW. This, in turn, contributes to an underestimation of the increase in atmospheric pCO_2 during the early deglaciation.

During the BA and YD periods, large changes in the AMOC caused bipolar climate changes, altering not only the distributions of temperature and salinity, but also affecting the vertical gradients of DIC and alkalinity. The net effects of those changes on atmospheric pCO_2 appear to be mutually offsetting, with slight decrease during the BA and increase during the YD. It was found that not only the change in $pCO_2{}^{os}$ due to changes in the amount of regenerated carbon accumulated by biological processes, but also the change in $pCO_2{}^{os}$ due to changes in alkalinity contributed more significantly during the BA and lowering atmospheric pCO_2.

To simulate transient changes in the carbon cycle, model biases, experimental settings, and the models themselves need to be improved to more realistically capture dynamical and biogeochemical changes in the atmosphere and ocean. Further research is needed to clarify what processes contribute to changes in the ocean carbon cycle at different time scales in each ocean basin. We emphasize that the analysis of carbon isotope variations provides insights into past carbon cycle dynamics and contributes to a better understanding of glacial-interglacial variations in the ocean carbon cycle.

Code and data availability.   COCO is an ocean component of MIROC and the code of COCO4 is included as a part of MIROCES2L. The source code of MIROC-ES2L can be obtained from https://doi.org/10.5281/zenodo.3893386 (Ohgaito et al., 2021).

Author contributions.   H.K. and A.O. designed the research. H.K. conducted the numerical experiments with help from T.O. H.K. performed the analysis and wrote the paper. A.O. and A.A.O. obtained funding and supervised the study. All authors discussed the results and commented on the manuscript.

Competing interests.   The authors declare that they have no competing interests.

445

Acknowledgements. This work was supported by JSPS KAKENHI Grant Numbers JP17H06104, JP17H06323, JP19H01963, and JP21K13990.
We thank James Buxton MSc, from Edanz (https://jp.edanz.com/ac), for editing a draft of this manuscript.

References

Ai, X. E., Studer, A. S., Sigman, D. M., Martínez-García, A., Fripiat, F., Thöle, L. M., Michel, E., Gottschalk, J., Arnold, L., Moretti, S., Schmitt, M., Oleynik, S., Jaccard, S. L., and Haug, G. H.: Southern Ocean upwelling, Earth's obliquity, and glacial-interglacial atmospheric CO_2 change, Science, 370, 1348–1352, https://doi.org/10.1126/science.abd2115, 2020.

Anderson, R. F., Ali, S., Bradtmiller, L. I., Nielsen, S. H. H., Fleisher, M. Q., Anderson, B. E., and Burckle, L. H.: Wind-Driven Upwelling in the Southern Ocean and the Deglacial Rise in Atmospheric CO_2, Science, 323, 1443–1448, https://doi.org/10.1126/science.1167441, 2009.

Annan, J. D., Hargreaves, J. C., and Mauritsen, T.: A new global surface temperature reconstruction for the Last Glacial Maximum, Climate of the Past, 18, 1883–1896, https://doi.org/10.5194/cp-18-1883-2022, 2022.

Barnola, J. M., Raynaud, D., Korotkevich, Y. S., and Lorius, C.: Vostok ice core provides 160, 000-year record of atmospheric CO_2, Nature, 329, 408–414, https://doi.org/10.1038/329408a0, 1987.

Bauska, T. K., Marcott, S. A., and Brook, E. J.: Abrupt changes in the global carbon cycle during the last glacial period, Nature Geoscience, 14, 91–96, https://doi.org/10.1038/s41561-020-00680-2, 2021.

Bereiter, B., Eggleston, S., Schmitt, J., Nehrbass-Ahles, C., Stocker, T. F., Fischer, H., Kipfstuhl, S., and Chappellaz, J.: Revision of the EPICA Dome C CO_2 record from 800 to 600 kyr before present, Geophysical Research Letters, 42, 542–549, https://doi.org/10.1002/2014gl061957, 2015.

Bolton, C. T., Lawrence, K. T., Gibbs, S. J., Wilson, P. A., and Herbert, T. D.: Biotic and geochemical evidence for a global latitudinal shift in ocean biogeochemistry and export productivity during the late Pliocene, Earth and Planetary Science Letters, 308, 200–210, https://doi.org/10.1016/j.epsl.2011.05.046, 2011.

Bouttes, N., Paillard, D., Roche, D. M., Waelbroeck, C., Kageyama, M., Lourantou, A., Michel, E., and Bopp, L.: Impact of oceanic processes on the carbon cycle during the last termination, Climate of the Past, 8, 149–170, https://doi.org/10.5194/cp-8-149-2012, 2012a.

Bouttes, N., Roche, D. M., and Paillard, D.: Systematic study of the impact of fresh water fluxes on the glacial carbon cycle, Climate of the Past, 8, 589–607, https://doi.org/10.5194/cp-8-589-2012, 2012b.

Bouttes, N., Lhardy, F., Quiquet, A., Paillard, D., Goosse, H., and Roche, D. M.: Deglacial climate changes as forced by different ice sheet reconstructions, Climate of the Past, 19, 1027–1042, https://doi.org/10.5194/cp-19-1027-2023, 2023.

Broecker, W. S. and Maier-Reimer, E.: The influence of air and sea exchange on the carbon isotope distribution in the sea, Global Biogeochemical Cycles, 6, 315–320, https://doi.org/10.1029/92gb01672, 1992.

Brovkin, V., Ganopolski, A., Archer, D., and Munhoven, G.: Glacial CO_2 cycle as a succession of key physical and biogeochemical processes, Climate of the Past, 8, 251–264, https://doi.org/10.5194/cp-8-251-2012, 2012.

Chase, Z., Anderson, R. F., Fleisher, M. Q., and Kubik, P. W.: Accumulation of biogenic and lithogenic material in the Pacific sector of the Southern Ocean during the past 40, 000 years, Deep Sea Research Part II: Topical Studies in Oceanography, 50, 799–832, https://doi.org/10.1016/s0967-0645(02)00595-7, 2003.

Chikamoto, M. O., Menviel, L., Abe-Ouchi, A., Ohgaito, R., Timmermann, A., Okazaki, Y., Harada, N., Oka, A., and Mouchet, A.: Variability in North Pacific intermediate and deep water ventilation during Heinrich events in two coupled climate models, Deep Sea Research Part II: Topical Studies in Oceanography, 61-64, 114–126, https://doi.org/10.1016/j.dsr2.2011.12.002, 2012.

Conkright, M. E., Garcia, H. E., O'Brien, T. D., Locarnini, R. A., Boyer, T. P., Stephens, C., and Antonov, J. I.: World Ocean Atlas 2001, vol. 4, Nutrients, NOAA Atlas NESDIS, vol. 52, p. 392 pp., NOAA, Silver Spring, Md., 2002.

485   Dome Fuji Ice Core Project Members: State dependence of climatic instability over the past 720,000 years from Antarctic ice cores and climate modeling, Science Advances, 3, e1600 446, https://doi.org/10.1126/sciadv.1600446, 2017.

Ganopolski, A. and Brovkin, V.: Simulation of climate, ice sheets and CO_2 evolution during the last four glacial cycles with an Earth system model of intermediate complexity, Climate of the Past, 13, 1695–1716, https://doi.org/10.5194/cp-13-1695-2017, 2017.

Ganopolski, A. and Roche, D. M.: On the nature of lead–lag relationships during glacial–interglacial climate transitions, Quaternary Science
490   Reviews, 28, 3361–3378, https://doi.org/10.1016/j.quascirev.2009.09.019, 2009.

Gottschalk, J., Battaglia, G., Fischer, H., Frölicher, T. L., Jaccard, S. L., Jeltsch-Thömmes, A., Joos, F., Köhler, P., Meissner, K. J., Menviel, L., Nehrbass-Ahles, C., Schmitt, J., Schmittner, A., Skinner, L. C., and Stocker, T. F.: Mechanisms of millennial-scale atmospheric CO_2 change in numerical model simulations, Quaternary Science Reviews, 220, 30–74, https://doi.org/10.1016/j.quascirev.2019.05.013, 2019.

Gray, W. R., de Lavergne, C., Wills, R. C. J., Menviel, L., Spence, P., Holzer, M., Kageyama, M., and Michel, E.: Poleward Shift in
495   the Southern Hemisphere Westerly Winds Synchronous With the Deglacial Rise in CO_2, Paleoceanography and Paleoclimatology, 38, e2023PA004 666, https://doi.org/10.1029/2023pa004666, 2023.

Gu, S., Liu, Z., Oppo, D. W., Lynch-Stieglitz, J., Jahn, A., Zhang, J., Lindsay, K., and Wu, L.: Remineralization dominating the $\delta^{13}C$ decrease in the mid-depth Atlantic during the last deglaciation, Earth and Planetary Science Letters, 571, 117 106, https://doi.org/10.1016/j.epsl.2021.117106, 2021.

500   Hasumi, H.: CCSR Rep. 25, chap. CCSR Ocean Component Model (COCO) Version 4.0, p. 103 pp., Center for Climate System Research, Univ. of Tokyo, Japan, 2006.

He, F., Shakun, J. D., Clark, P. U., Carlson, A. E., Liu, Z., Otto-Bliesner, B. L., and Kutzbach, J. E.: Northern Hemisphere forcing of Southern Hemisphere climate during the last deglaciation, Nature, 494, 81–85, https://doi.org/10.1038/nature11822, 2013.

Howe, J. N. W., Piotrowski, A. M., Noble, T. L., Mulitza, S., Chiessi, C. M., and Bayon, G.: North Atlantic Deep Water Production during
505   the Last Glacial Maximum, Nature Communications, 7, https://doi.org/10.1038/ncomms11765, 2016.

Ivanovic, R. F., Gregoire, L. J., Kageyama, M., Roche, D. M., Valdes, P. J., Burke, A., Drummond, R., Peltier, W. R., and Tarasov, L.: Transient climate simulations of the deglaciation 21–9 thousand years before present (version 1) – PMIP4 Core experiment design and boundary conditions, Geoscientific Model Development, 9, 2563–2587, https://doi.org/10.5194/gmd-9-2563-2016, 2016.

Ivanovic, R. F., Gregoire, L. J., Burke, A., Wickert, A. D., Valdes, P. J., Ng, H. C., Robinson, L. F., McManus, J. F., Mitrovica, J. X., Lee, L.,
510   and Dentith, J. E.: Acceleration of Northern Ice Sheet Melt Induces AMOC Slowdown and Northern Cooling in Simulations of the Early Last Deglaciation, Paleoceanography and Paleoclimatology, 33, 807–824, https://doi.org/10.1029/2017pa003308, 2018.

Jochum, M., Chase, Z., Nuterman, R., Pedro, J., Rasmussen, S., Vettoretti, G., and Zheng, P.: Carbon Fluxes during Dansgaard–Oeschger Events as Simulated by an Earth System Model, Journal of Climate, 35, 5745–5758, https://doi.org/10.1175/jcli-d-21-0713.1, 2022.

Jouzel, J., Masson-Delmotte, V., Cattani, O., Dreyfus, G., Falourd, S., Hoffmann, G., Minster, B., Nouet, J., Barnola, J. M., Chappellaz,
515   J., Fischer, H., Gallet, J. C., Johnsen, S., Leuenberger, M., Loulergue, L., Luethi, D., Oerter, H., Parrenin, F., Raisbeck, G., Raynaud, D., Schilt, A., Schwander, J., Selmo, E., Souchez, R., Spahni, R., Stauffer, B., Steffensen, J. P., Stenni, B., Stocker, T. F., Tison, J. L., Werner, M., and Wolff, E. W.: Orbital and Millennial Antarctic Climate Variability over the Past 800,000 Years, Science, 317, 793–796, https://doi.org/10.1126/science.1141038, 2007.

K-1 Model Developers: K-1 Tech. Rep. 1, chap. K-1 Coupled GCM (MIROC) Description, p. 34 pp., Center for Climate System Research,
520   Univ. of Tokyo, Japan, 2004.

Kapsch, M.-L., Mikolajewicz, U., Ziemen, F., and Schannwell, C.: Ocean Response in Transient Simulations of the Last Deglacia-
tion Dominated by Underlying Ice-Sheet Reconstruction and Method of Meltwater Distribution, Geophysical Research Letters, 49,
https://doi.org/10.1029/2021gl096767, 2022.

525 Kawasaki, T., Matsumura, Y., and Hasumi, H.: Deep water pathways in the North Pacific Ocean revealed by Lagrangian particle tracking,
Scientific Reports, 12, https://doi.org/10.1038/s41598-022-10080-8, 2022.

Key, R. M., Kozyr, A., Sabine, C. L., Lee, K., Wanninkhof, R., Bullister, J. L., Feely, R. A., Millero, F. J., Mordy, C., and Peng, T.-H.: A
global ocean carbon climatology: Results from Global Data Analysis Project (GLODAP), Global Biogeochemical Cycles, 18, GB4031,
https://doi.org/10.1029/2004gb002247, 2004.

Kobayashi, H., Oka, A., Yamamoto, A., and Abe-Ouchi, A.: Glacial carbon cycle changes by Southern Ocean processes with sedimentary
530 amplification, Science Advances, 7, https://doi.org/10.1126/sciadv.abg7723, 2021.

Kohfeld, K. E. and Chase, Z.: Controls on deglacial changes in biogenic fluxes in the North Pacific Ocean, Quaternary Science Reviews, 30,
3350–3363, https://doi.org/10.1016/j.quascirev.2011.08.007, 2011.

Kurahashi-Nakamura, T., Paul, A., and Losch, M.: Dynamical reconstruction of the global ocean state during the Last Glacial Maximum,
Paleoceanography, 32, 326–350, https://doi.org/10.1002/2016pa003001, 2017.

535 Li, C., Clementi, V. J., Bova, S. C., Rosenthal, Y., Childress, L. B., Wright, J. D., and and, Z. J.: The Sediment Green-Blue
Color Ratio as a Proxy for Biogenic Silica Productivity Along the Chilean Margin, Geochemistry, Geophysics, Geosystems, 23,
https://doi.org/10.1029/2022gc010350, 2022.

Liu, Z., Otto-Bliesner, B. L., He, F., Brady, E. C., Tomas, R., Clark, P. U., Carlson, A. E., Lynch-Stieglitz, J., Curry, W., Brook, E., Erickson,
D., Jacob, R., Kutzbach, J., and Cheng, J.: Transient Simulation of Last Deglaciation with a New Mechanism for Bølling-Allerød Warming,
540 Science, 325, 310–314, https://doi.org/10.1126/science.1171041, 2009.

Locarnini, R. A., O'Brien, T. D., Garcia, H. E., Antonov, J. I., Boyer, T. P., Conkright, M. E., and Stephens, C.: World Ocean Atlas 2001,
vol. 3, Oxygen, NOAA Atlas NESDIS, vol. 51, p. 286 pp., NOAA, Silver Spring, Md., 2002.

Lunt, D. J., Williamson, M. S., Valdes, P. J., Lenton, T. M., and Marsh, R.: Comparing transient, accelerated, and equilibrium simulations of
the last 30 000 years with the GENIE-1 model, Climate of the Past, 2, 221–235, https://doi.org/10.5194/cp-2-221-2006, 2006.

545 Lüthi, D., Floch, M. L., Bereiter, B., Blunier, T., Barnola, J.-M., Siegenthaler, U., Raynaud, D., Jouzel, J., Fischer, H., Kawamura, K.,
and Stocker, T. F.: High-resolution carbon dioxide concentration record 650,000–800,000 years before present, Nature, 453, 379–382,
https://doi.org/10.1038/nature06949, 2008.

Maier, E., Méheust, M., Abelmann, A., Gersonde, R., Chapligin, B., Ren, J., Stein, R., Meyer, H., and Tiedemann, R.: Deglacial subarctic
Pacific surface water hydrography and nutrient dynamics and links to North Atlantic climate variability and atmospheric CO_2, Paleo-
550 ceanography, 30, 949–968, https://doi.org/10.1002/2014pa002763, 2015.

Marcott, S. A., Bauska, T. K., Buizert, C., Steig, E. J., Rosen, J. L., Cuffey, K. M., Fudge, T. J., Severinghaus, J. P., Ahn, J., Kalk, M. L.,
McConnell, J. R., Sowers, T., Taylor, K. C., White, J. W. C., and Brook, E. J.: Centennial-scale changes in the global carbon cycle during
the last deglaciation, Nature, 514, 616–619, https://doi.org/10.1038/nature13799, 2014.

MARGO Project Members: Constraints on the magnitude and patterns of ocean cooling at the Last Glacial Maximum, Nature Geoscience,
555 2, 127–132, https://doi.org/10.1038/ngeo411, 2009.

Mariotti, V., Paillard, D., Bopp, L., Roche, D. M., and Bouttes, N.: A coupled model for carbon and radiocarbon evolution during the last
deglaciation, Geophysical Research Letters, 43, 1306–1313, https://doi.org/10.1002/2015gl067489, 2016.

Martin, J. H.: Glacial-interglacial CO_2 change: The Iron Hypothesis, Paleoceanography, 5, 1–13, https://doi.org/10.1029/pa005i001p00001, 1990.

560 Martínez-García, A., Sigman, D. M., Ren, H., Anderson, R. F., Straub, M., Hodell, D. A., Jaccard, S. L., Eglinton, T. I., and Haug, G. H.: Iron Fertilization of the Subantarctic Ocean During the Last Ice Age, Science, 343, 1347–1350, https://doi.org/10.1126/science.1246848, 2014.

McManus, J. F., Francois, R., Gherardi, J.-M., Keigwin, L. D., and Brown-Leger, S.: Collapse and rapid resumption of Atlantic meridional circulation linked to deglacial climate changes, Nature, 428, 834–837, https://doi.org/10.1038/nature02494, 2004.

565 Menviel, L., Timmermann, A., Mouchet, A., and Timm, O.: Climate and marine carbon cycle response to changes in the strength of the Southern Hemispheric westerlies, Paleoceanography, 23, https://doi.org/10.1029/2008pa001604, 2008.

Menviel, L., Timmermann, A., Timm, O. E., and Mouchet, A.: Deconstructing the Last Glacial termination: the role of millennial and orbital-scale forcings, Quaternary Science Reviews, 30, 1155–1172, https://doi.org/10.1016/j.quascirev.2011.02.005, 2011.

Menviel, L., Joos, F., and Ritz, S.: Simulating atmospheric CO_2, ^{13}C and the marine carbon cycle during the Last Glacial–Interglacial cycle: 570 possible role for a deepening of the mean remineralization depth and an increase in the oceanic nutrient inventory, Quaternary Science Reviews, 56, 46–68, https://doi.org/10.1016/j.quascirev.2012.09.012, 2012.

Menviel, L., England, M. H., Meissner, K. J., Mouchet, A., and Yu, J.: Atlantic-Pacific seesaw and its role in outgassing CO_2 during Heinrich events, Paleoceanography, 29, 58–70, https://doi.org/10.1002/2013pa002542, 2014.

Menviel, L., Yu, J., Joos, F., Mouchet, A., Meissner, K. J., and England, M. H.: Poorly ventilated deep ocean at the Last Glacial Maximum 575 inferred from carbon isotopes: A data-model comparison study, Paleoceanography, 32, 2–17, https://doi.org/10.1002/2016pa003024, 2017.

Menviel, L., Spence, P., Yu, J., Chamberlain, M. A., Matear, R. J., Meissner, K. J., and England, M. H.: Southern Hemisphere westerlies as a driver of the early deglacial atmospheric CO2 rise, Nature Communications, 9, https://doi.org/10.1038/s41467-018-04876-4, 2018.

Millero, F. J.: Thermodynamics of the carbon dioxide system in the oceans, Geochimica et Cosmochimica Acta, 59, 661–677, https://doi.org/10.1016/0016-7037(94)00354-o, 1995.

580 Muglia, J., Skinner, L. C., and Schmittner, A.: Weak overturning circulation and high Southern Ocean nutrient utilization maximized glacial ocean carbon, Earth and Planetary Science Letters, 496, 47–56, https://doi.org/10.1016/j.epsl.2018.05.038, 2018.

Muglia, J., Mulitza, S., Repschläger, J., Schmittner, A., Lembke-Jene, L., Lisiecki, L., Mix, A., Saraswat, R., Sikes, E., Waelbroeck, C., Gottschalk, J., Lippold, J., Lund, D., Martinez-Mendez, G., Michel, E., Muschitiello, F., Naik, S., Okazaki, Y., Stott, L., Voelker, A., and Zhao, N.: A global synthesis of high-resolution stable isotope data from benthic foraminifera of the last deglaciation, Scientific Data, 10, 585 https://doi.org/10.1038/s41597-023-02024-2, 2023.

Ng, H. C., Robinson, L. F., McManus, J. F., Mohamed, K. J., Jacobel, A. W., Ivanovic, R. F., Gregoire, L. J., and Chen, T.: Coherent deglacial changes in western Atlantic Ocean circulation, Nature Communications, 9, https://doi.org/10.1038/s41467-018-05312-3, 2018.

Obase, T. and Abe-Ouchi, A.: Abrupt Bölling-Alleröd Warming Simulated under Gradual Forcing of the Last Deglaciation, Geophysical Research Letters, 46, 11 397–11 405, https://doi.org/10.1029/2019gl084675, 2019.

590 Obase, T., Abe-Ouchi, A., and Saito, F.: Abrupt climate changes in the last two deglaciations simulated with different Northern ice sheet discharge and insolation, Scientific Reports, 11, https://doi.org/10.1038/s41598-021-01651-2, 2021.

Obase, T., Menviel, L., Abe-Ouchi, A., Vadsaria, T., Ivanovic, R., Snoll, B., Sherriff-Tadano, S., Valdes, P. J., Gregoire, L., Kapsch, M.-L., Mikolajewicz, U., Bouttes, N., Roche, D., Lhardy, F., He, C., Otto-Bliesner, B., and Liu, Z.: Multi-model assessment of the deglacial climatic evolution at high southern latitudes, Climate of the Past, Discuss, 2023.

595 Ohgaito, R., Yamamoto, A., Hajima, T., O'ishi, R., Abe, M., Tatebe, H., Abe-Ouchi, A., and Kawamiya, M.: PMIP4 experiments using MIROC-ES2L Earth system model, Geoscientific Model Development, 14, 1195–1217, https://doi.org/10.5194/gmd-14-1195-2021, 2021.

Oka, A. and Niwa, Y.: Pacific deep circulation and ventilation controlled by tidal mixing away from the sea bottom, Nature Communications, 4, https://doi.org/10.1038/ncomms3419, 2013.

Okazaki, Y., Timmermann, A., Menviel, L., Harada, N., Abe-Ouchi, A., Chikamoto, M. O., Mouchet, A., and Asahi, H.: Deepwater Formation
600 in the North Pacific During the Last Glacial Termination, Science, 329, 200–204, https://doi.org/10.1126/science.1190612, 2010.

O'Leary, M. H.: Carbon isotope fractionation in plants, Phytochemistry, 20, 553–567, https://doi.org/10.1016/0031-9422(81)85134-5, 1981.

Parekh, P., Follows, M. J., and Boyle, E. A.: Decoupling of iron and phosphate in the global ocean, Global Biogeochemical Cycles, 19, GB2020, https://doi.org/10.1029/2004gb002280, 2005.

Paul, A., Mulitza, S., Stein, R., and Werner, M.: A global climatology of the ocean surface during the Last Glacial Maximum mapped on a
605 regular grid (GLOMAP), Climate of the Past, 17, 805–824, https://doi.org/10.5194/cp-17-805-2021, 2021.

Petit, J. R., Jouzel, J., Raynaud, D., Barkov, N. I., Barnola, J.-M., Basile, I., Bender, M., Chappellaz, J., Davis, M., Delaygue, G., Delmotte, M., Kotlyakov, V. M., Legrand, M., Lipenkov, V. Y., Lorius, C., PÉpin, L., Ritz, C., Saltzman, E., and Stievenard, M.: Climate and atmospheric history of the past 420, 000 years from the Vostok ice core, Antarctica, Nature, 399, 429–436, https://doi.org/10.1038/20859, 1999.

610 Pöppelmeier, F., Jeltsch-Thömmes, A., Lippold, J., Joos, F., and Stocker, T. F.: Multi-proxy constraints on Atlantic circulation dynamics since the last ice age, Nature Geoscience, 16, 349–356, https://doi.org/10.1038/s41561-023-01140-3, 2023.

Rae, J. W. B., Sarnthein, M., Foster, G. L., Ridgwell, A., Grootes, P. M., and Elliott, T.: Deep water formation in the North Pacific and deglacial CO_2 rise, Paleoceanography, 29, 645–667, https://doi.org/10.1002/2013pa002570, 2014.

Rafter, P. A., Gray, W. R., Hines, S. K., Burke, A., Costa, K. M., Gottschalk, J., Hain, M. P., Rae, J. W., Southon, J. R., Walczak, M. H., Yu, J.,
615 Adkins, J. F., and DeVries, T.: Global reorganization of deep-sea circulation and carbon storage after the last ice age, Science Advances, 8, https://doi.org/10.1126/sciadv.abq5434, 2022.

Schmitt, J., Schneider, R., Elsig, J., Leuenberger, D., Lourantou, A., Chappellaz, J., Köhler, P., Joos, F., Stocker, T. F., Leuenberger, M., and Fischer, H.: Carbon isotope constraints on the deglacial CO_2 rise from ice cores, Science, 336, 711–714, https://doi.org/10.1126/science.1217161, 2012.

620 Schmittner, A. and Galbraith, E. D.: Glacial greenhouse-gas fluctuations controlled by ocean circulation changes, Nature, 456, 373–376, https://doi.org/10.1038/nature07531, 2008.

Schmittner, A. and Lund, D. C.: Early deglacial Atlantic overturning decline and its role in atmospheric CO_2 rise inferred from carbon isotopes (δ^{13}C), Climate of the Past, 11, 135–152, https://doi.org/10.5194/cp-11-135-2015, 2015.

Schmittner, A., Gruber, N., Mix, A. C., Key, R. M., Tagliabue, A., and Westberry, T. K.: Biology and air–sea gas exchange controls on the
625 distribution of carbon isotope ratios (δ^{13}C) in the ocean, Biogeosciences, 10, 5793–5816, https://doi.org/10.5194/bg-10-5793-2013, 2013.

Sherriff-Tadano, S., Abe-Ouchi, A., Yoshimori, M., Ohgaito, R., Vadsaria, T., Chan, W.-L., Hotta, H., Kikuchi, M., Kodama, T., Oka, A., and Suzuki, K.: Southern Ocean Surface Temperatures and Cloud Biases in Climate Models Connected to the Representation of Glacial Deep Ocean Circulation, Journal of Climate, 36, 3849–3866, https://doi.org/10.1175/jcli-d-22-0221.1, 2023.

Siegenthaler, U., Stocker, T. F., Monnin, E., Lüthi, D., Schwander, J., Stauffer, B., Raynaud, D., Barnola, J.-M., Fischer, H., Masson-
630 Delmotte, V., and Jouzel, J.: Stable Carbon Cycle–Climate Relationship During the Late Pleistocene, Science, 310, 1313–1317, https://doi.org/10.1126/science.1120130, 2005.

Sigman, D. M., Fripiat, F., Studer, A. S., Kemeny, P. C., Martínez-García, A., Hain, M. P., Ai, X., Wang, X., Ren, H., and Haug, G. H.: The Southern Ocean during the ice ages: A review of the Antarctic surface isolation hypothesis, with comparison to the North Pacific, Quaternary Science Reviews, 254, 106 732, https://doi.org/10.1016/j.quascirev.2020.106732, 2021.

635 Sikes, E. L., Umling, N. E., Allen, K. A., Ninnemann, U. S., Robinson, R. S., Russell, J. L., and Williams, T. J.: Southern Ocean glacial conditions and their influence on deglacial events, Nature Reviews Earth & Environment, 4, 454–470, https://doi.org/10.1038/s43017-023-00436-7, 2023.

Snoll, B., Ivanovic, R., Gregoire, L., Sherriff-Tadano, S., Menviel, L., Obase, T., Abe-Ouchi, A., Bouttes, N., He, C., He, F., Kapsch, M., Mikolajewicz, U., Muglia, J., and Valdes, P.: A multi-model assessment of the early last deglaciation (PMIP4 LDv1): The meltwater 640 paradox reigns supreme, https://doi.org/10.5194/egusphere-2023-1802, 2023.

Stein, K., Timmermann, A., Kwon, E. Y., and Friedrich, T.: Timing and magnitude of Southern Ocean sea ice/carbon cycle feedbacks, Proceedings of the National Academy of Sciences, 117, 4498–4504, https://doi.org/10.1073/pnas.1908670117, 2020.

Studer, A. S., Sigman, D. M., Martínez-García, A., Benz, V., Winckler, G., Kuhn, G., Esper, O., Lamy, F., Jaccard, S. L., Wacker, L., Oleynik, S., Gersonde, R., and Haug, G. H.: Antarctic Zone nutrient conditions during the last two glacial cycles, Paleoceanography, 30, 845–862, 645 https://doi.org/10.1002/2014pa002745, 2015.

Stuiver, M., Quay, P. D., and Ostlund, H. G.: Abyssal Water Carbon-14 Distribution and the Age of the World Oceans, Science, 219, 849–851, https://doi.org/10.1126/science.219.4586.849, 1983.

Takemura, T.: Simulation of climate response to aerosol direct and indirect effects with aerosol transport-radiation model, Journal of Geophysical Research, 110, D02 202, https://doi.org/10.1029/2004jd005029, 2005.

650 Thiagarajan, N. and McManus, J. F.: Productivity and sediment focusing in the Eastern Equatorial Pacific during the last 30, 000 years, Deep Sea Research Part I: Oceanographic Research Papers, 147, 100–110, https://doi.org/10.1016/j.dsr.2019.03.007, 2019.

Tierney, J. E., Zhu, J., King, J., Malevich, S. B., Hakim, G. J., and Poulsen, C. J.: Glacial cooling and climate sensitivity revisited, Nature, 584, 569–573, https://doi.org/10.1038/s41586-020-2617-x, 2020.

Timm, O. and Timmermann, A.: Simulation of the Last 21 000 Years Using Accelerated Transient Boundary Conditions, Journal of Climate, 655 20, 4377–4401, https://doi.org/10.1175/jcli4237.1, 2007.

Tschumi, T., Joos, F., Gehlen, M., and Heinze, C.: Deep ocean ventilation, carbon isotopes, marine sedimentation and the deglacial CO_2 rise, Climate of the Past, 7, 771–800, https://doi.org/10.5194/cp-7-771-2011, 2011.

Weber, M. E.: Antiphased dust deposition and productivity in the Antarctic Zone over 1.5 million years, https://doi.org/10.1594/PANGAEA.939650, 2021.

660 Wilmes, S.-B., Green, J. A. M., and Schmittner, A.: Enhanced vertical mixing in the glacial ocean inferred from sedimentary carbon isotopes, Communications Earth & Environment, 2, https://doi.org/10.1038/s43247-021-00239-y, 2021.

Zhao, N., Marchal, O., Keigwin, L., Amrhein, D., and Gebbie, G.: A Synthesis of Deglacial Deep-Sea Radiocarbon Records and Their (In)Consistency With Modern Ocean Ventilation, Paleoceanography and Paleoclimatology, 33, 128–151, https://doi.org/10.1002/2017pa003174, 2018.
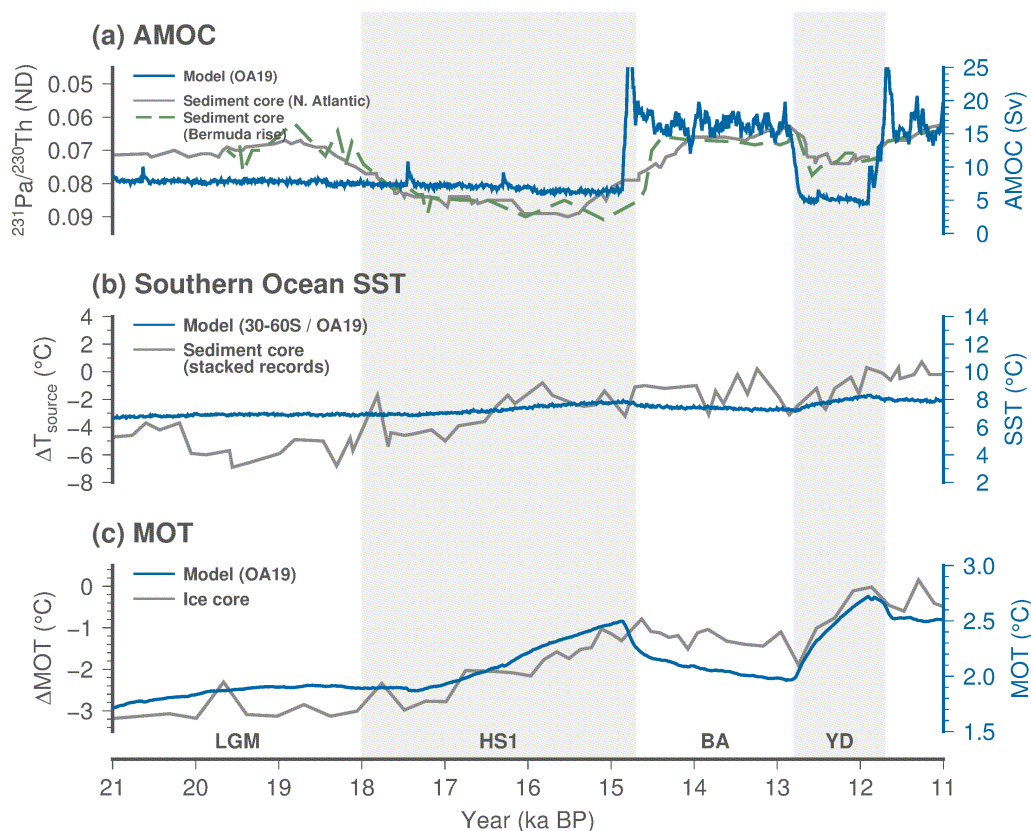
Figure 1. (a) Deglacial changes in the maximum volume transport of the Atlantic Meridional Overturning Circulation (AMOC; Sverdrup) with ^{231}Pa/^{230}Th reconstructed from sediment core data at the Bermuda Rise (McManus et al., 2004) and compiled sediment core data in the North Atlantic (Ng et al., 2018). (b) Deglacial changes in sea surface temperature (SST) in the Southern Ocean (°C) and the difference in SST from the present day (ΔT$_{source}$) (Uemura et al., 2018). (c) Deglacial changes in global mean ocean temperature (MOT; °C) and the difference in MOT from the present day ("Mix" of Bereiter et al., 2018). The model output computed by the AOGCM (OA19) (Obase and Abe-Ouchi, 2019), shown by blue lines, is compared to reconstructions from geological data, shown by gray lines. The right axes relate to the model output and the left axes relate to the reconstructions.
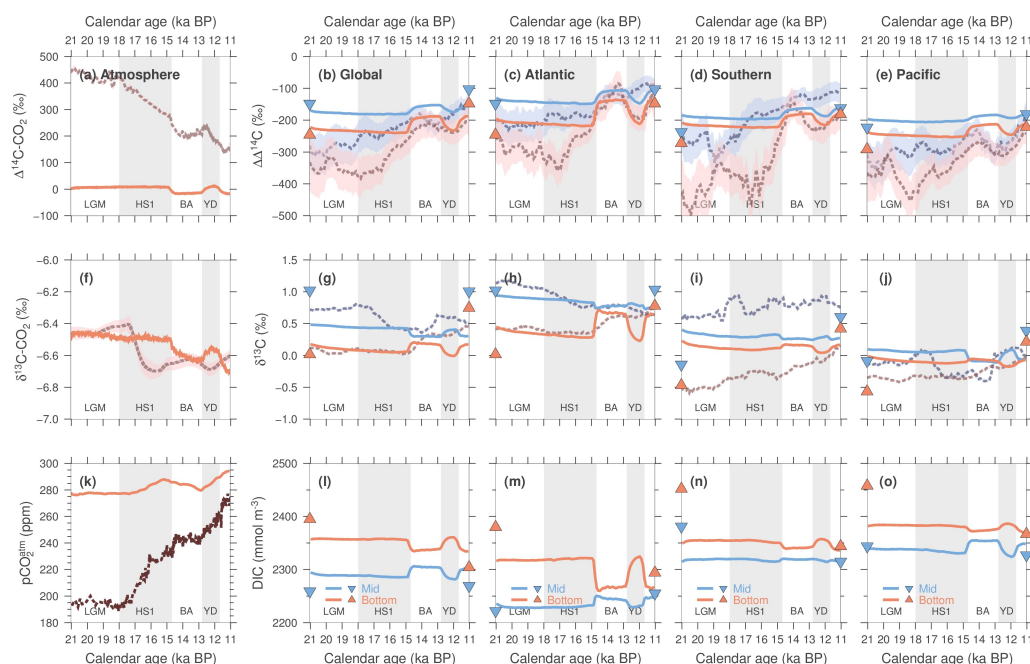
Figure 2. (a) Deglacial changes in Δ^{14}C-CO$_2$ (‰) in the atmosphere (solid line) with the reconstruction of IntCal20 (dashed line; Reimer et al., 2020). (b–e) Deglacial changes in $\Delta\Delta^{14}$C (‰), difference in Δ^{14}C (‰) between the ocean and the atmosphere, averaged in the mid-depth (500–2000 m; blue solid line) and deep global ocean (2000–5500 m; red solid line), Atlantic Ocean (40°S–90°N), Pacific Ocean (40°S–90°N), and the Southern Ocean (90°–40°S) with compiled sediment core data (dashed line) of Rafter et al. (2022). (f) Deglacial changes in δ^{13}C-CO$_2$ (‰) in the atmosphere (solid line) with the reconstruction (dashed line; Schmitt et al., 2012). (g–i) Same as (b–e), respectively, except for δ^{13}C (‰) with compiled sediment core data of Muglia et al. (2023). (k) Deglacial changes in atmospheric pCO$_2$ (ppm; solid line) with ice core data (dashed line; Bauska et al., 2021). (l–o) Same as (b–e), respectively, except for dissolved inorganic carbon (DIC; mmol m^{-3}). The triangles represent the values reported in Kobayashi et al. (2021), with the output of PI_sed plotted at the time of 11 kaBP and the output of LGM_all plotted at the time of 21 kaBP.
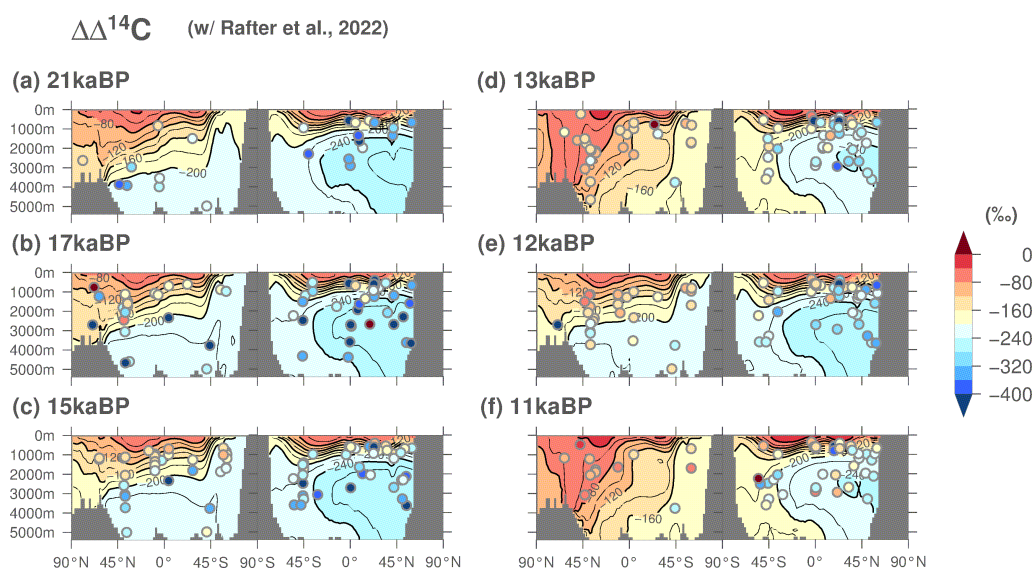
Figure 3. Oceanic zonal mean distribution of $\Delta\Delta^{14}$C (‰), which represents the difference in Δ^{14}C between the ocean and the atmosphere, during key periods of the last deglaciation in the Atlantic and Pacific oceans. The specific periods of interest include (a) the Last Glacial Maximum (21 kaBP), (b) Heinrich Stadial 1 (17 kaBP), (c) just before the Bølling-Allerød (BA) transition (15 kaBP), (d) the Bølling-Allerød (BA) warm period (13 kaBP), (e) the Younger Dryas (12 kaBP) and (f) the Holocene (11 kaBP). The contour interval is 40‰. The sediment core records used in the figure are compiled in Rafter et al. (2022). Model results are averaged over 200 years, i.e., 100 years before and after each target year. However, for 21 kaBP, the average is taken from results spanning 21.0–20.9 kaBP; for 11 kaBP, the average is taken from results spanning 11.1–11.0 kaBP. The figure also includes a compilation of sediment core records where reconstructed values are plotted for 250 years before and after the target year. The vertical section represents all data within the relevant ocean basins.
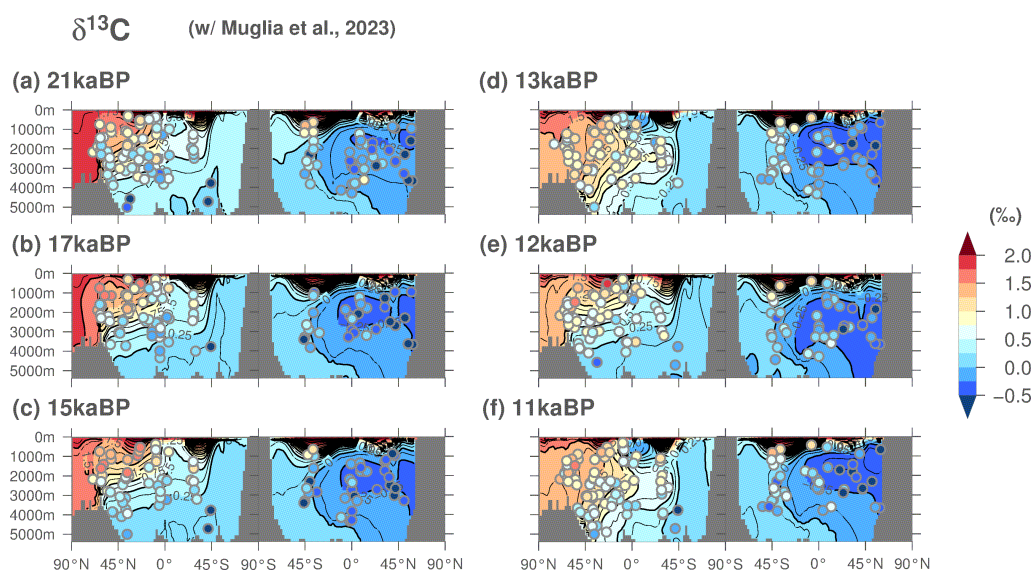
Figure 4. Oceanic zonal mean distribution of δ^{13}C (‰) during the last deglaciation in the Atlantic and Pacific oceans. The contour interval is 0.25‰. The sediment core records used in the figure are compiled in Muglia et al. (2023). The period over which the model output is averaged is 100 years before and after the year of interest. The reconstructed values are also plotted for 100 years before and after the year of interest.
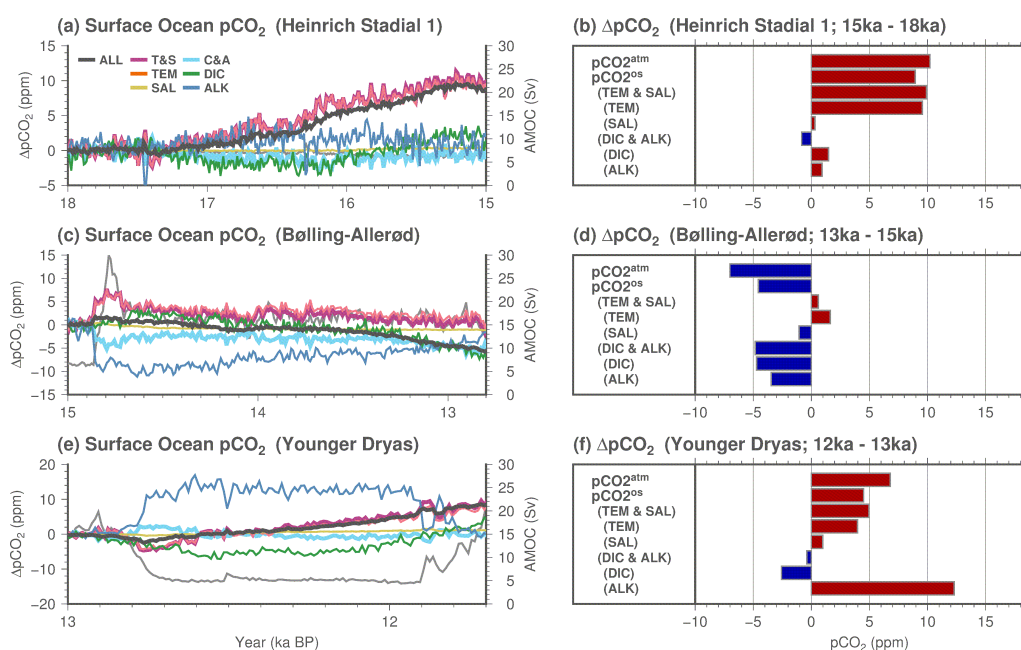
Figure 5. (a) Temporal changes in the partial pressure of sea surface CO_2 ($p\mathrm{CO_2}^{os}$; ppm; gray) during Heinrich Stadial 1 (HS1; differences between 18 and 15 kaBP). The contributions of changes in temperature and salinity (purple), temperature (red), salinity (yellow), dissolved inorganic carbon (DIC) and alkalinity (cyan), DIC (green), and alkalinity (blue) to the changes in $p\mathrm{CO_2}^{os}$ are shown. The thin gray line shows the time series of the AMOC strength. (b) Temporal changes in the partial pressure of atmospheric $p\mathrm{CO_2}$ and $p\mathrm{CO_2}^{os}$ (ppm) during HS1. The contributions of changes in temperature and salinity, temperature, salinity, DIC and alkalinity, DIC, and alkalinity to the changes in $p\mathrm{CO_2}^{os}$ are represented by different colored bars. (c) and (d) Similar to (a) and (b), respectively, but for the Bølling-Allerød (differences between 15 and 13 kaBP). (e) and (f) Similar to (a) and (b), respectively, but for the Younger Dryas (differences between 13 and 12 kaBP).